Journal of
Materials Chemistry C

Accepted Manuscript

Volume 4 | Number 1 | 7 January 2016 | Pages 1–224

Journal of
Materials Chemistry C

Materials for optical, magnetic and electronic devices
www.rsc.org/MaterialsC

ISSN 2050-7526

ROYAL SOCIETY OF CHEMISTRY

PAPER
Nguyễn T. K. Thanh, Xiaodi Su et al.
Fine-tuning of gold nanorod dimensions and plasmonic properties using the Hofmeister effects

175 YEARS

ROYAL SOCIETY OF CHEMISTRY

rsc.li/materials-c

Journal Name

ARTICLE

A 2-D π-π dimer model system to investigate structure-charge transfer relationships in rubrene

Sherlyn C. Jing,[a] Callum J. McHugh[b]* and Jesus Calvo-Castro[a]*

Rubrene (5,6,11,12-tetraphenyltetracene) is undoubtedly one of the the best performing organic charge transfer mediating materials, with experimentally determined mobilities up to 40 cm^2 V^{-1} s^{-1}. Consequently, there has been increasing interest by means of crystal engineering in trying to generate rubrene-based materials with analogous or even superior conducting properties. Often, experimental measurements are carried out in thin film architectures of these materials, where measured properties can be detrimentally impacted by device manufacture rather than intrinsic charge transfer properties of the material. The latter results in discarding potential good performers. To address these concerns, we report a two-dimensional model system that will allow researchers to predict charge transfer properties of their materials solely requiring the coordinates of the π-π stacking motifs. We envisaged this study to be of significant interest to the increasingly large community of material scientists devoted to the realisation of improved organic charge mediating materials and particularly to those engaged in exploiting rubrene-based architectures.

Introduction

In the last decades, material scientists have devoted their efforts in achieving optimum charge carrier mobilities in small organic conjugated systems. Among the plethora of systems that have been explored, rubrene (5,6,11,12-tetraphenyltetracene) has attracted an increasing interest, primarily due to the its exemplar field effect transistor properties, with experimentally determined values at room temperature of ca 20 cm^2 V^{-1} s^{-1} in single crystal organic field effect transistors (SC-OFET)[1] and a reported contact-free intrinsic mobility of ca 40 cm^2 V^{-1} s^{-1}.[2,3] Hitherto, three distinct polymorphs of rubrene have been reported, the monoclinic,[4] triclinic[4] and orthorhombic[5] rubrene forms. Whilst high mobilities have been experimentally determined for the orthorhombic form, the triclinic form exhibits values which are one order of magnitude lower and no evidence of semiconducting behaviour has been reported for the monoclinic form.[6] Although the mechanism responsible for these large mobilities is still a matter of significant debate, it is nowadays widely acknowledged that, over and above contributions such as interplanar distance, these remarkable experimental observations are associated to the supramolecular packing exhibited by orthorhombic rubrene, where the monomers self-assemble in a π-π

slipped co-facial fashion that conform to one-dimensional stacking motifs along the crystallographic a-axis. This supramolecular arrangement confers anisotropic charge transfer behaviour to rubrene and is further characterised by large structural overlap between the monomers resulting in associated strong wavefunction overlap, critically important in achieving large charge transfer integrals. Minimal intermonomer displacements along the short molecular axis (also referred to as roll angle) are also considered to play a significant role in ensuring large mobilities in rubrene systems due to enhanced wavefunction overlap.[7–9]
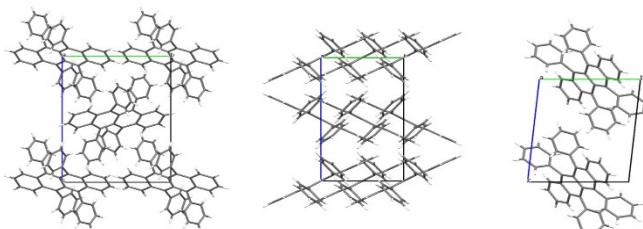
Figure 1. Capped sticks illustration of the crystal lattices for monoclinic (left), orthorhombic (centre) and triclinic (right) rubrene viewed along the a crystallographic axis.

More recently and inspired by these observations, crystal engineering has been exploited with a focus on improving the field-effect properties of rubrene derived materials by carrying out systematic substitutions on both the peripheral rings and the tetracene core that could ultimately result in different intermolecular slips along the long and short molecular axes and

a. Department of Clinical and Pharmaceutical Sciences. School of Life and Medical Sciences, University of Hertfordshire, Hatfield, AL10 9AB, UK.

b. School of Computing, Engineering and Physical Sciences, University of the West of Scotland, Paisley, PA1 2BE, UK..

*Email - j.calvo-castro@herts.ac.uk

Electronic Supplementary Information (ESI) available: Chemical structures and space-filled illustrations for all entries in Table 1 and 2. See

associated charge transfer integrals. Small conjugated organic materials have been reported to exhibit large sensitivity to small intermonomer displacements.[10–12] In some cases, the rationale behind such systematic structural alterations has been to bypass the chemical oxidation that is detrimental for charge transfer processes in rubrene and rubrene based systems.[13]

Underpinned by the experimentally acquired mobilities in rubrene, it is commonly acknowledged that organic single crystals (OSCs) play a crucial role in maximising the performance in optoelectronic devices due to their higher purity and structural order when compared to crystalline and amorphous thin films.[14–17] However, most reported experimental mobility data in the literature has been acquired employing thin film architectures where the presence of grain boundaries and defects are known to negatively influence the performance. As a consequence potentially good organic charge transfer mediating materials with charge transfer properties, which can equate or even improve upon existing ones, may be overlooked on the basis of poor preliminary data that might be ascribed to device manufacturing and not intrinsic material properties.[7,18]

Motivated by these outcomes, in the following we report a comprehensive analysis of dimeric intermolecular interactions and associated charge transfer integrals for all reported rubrene-based single crystal structures that conform to one-dimensional slipped cofacial π-π stacking motifs. Of particular note is the effect that systematic substitution bears on the intermonomer displacements along the long and short molecular axes as well as their effects on disrupting the highly sought-after planarity of the tetracene core. To further the understanding of substitution-induced changes to the intermonomer displacements and the associated effect on the charge transfer properties, we report for the first time a two-dimensional dimeric model system. The model was generated by simultaneously modifying the displacements along the long and short molecular axes and computing the associated intermolecular interactions and charge transfer integrals. Remarkably, the generated model system is able to qualitatively predict observed device mobility data. As a result, we anticipate the work presented herein to be of critical interest to the large community of material scientists devoted to the development of rubrene based materials and more broadly to all material scientists engaged in the engineering of crystalline systems for optoelectronic applications.

Experimental

Intermolecular interactions

Dimer pair binding energies were all calculated employing Truhlar's density functional M06-2X[19] at the 6-311G(d) level as implemented in Spartan 10 software.[20] Truhlar's density functional has shown to give good account of non-covalent intermolecular interactions in supramolecular organic conjugated systems.[10,11,21] All computed intermolecular interactions were corrected for Basis Set Superposition Error (BSSE) by means of the counterpoise method of Boys and Bernardi.[22]

Charge transfer integrals

Transfer integrals for hole (t_h) and electron (t_e) were computed by means of the energy splitting in dimer method for symmetric systems, with all dimer pairs investigated in this work being centrosymmetric. Within the framework of this method, t_h and t_e can be equated to half the splitting between the dimer HOMO/HOMO(-1) and LUMO/LUMO(+1) orbitals respectively. These calculations were carried out using Truhlar's density functional M06-2X at the 6-311G(d) level. We have previously reported[12] that whilst the use of ωB97X-D[23] density functional results in a 32% increase in the computed intermolecular interactions, the effect on the computer charge transfer integrals is negligible.

Inner-sphere reorganisation energies

The geometry of neutral (restricted) as well as radical anion/cation (unrestricted) tetracene and rubrene monomers were optimised by means of the density functional B3LYP[24–26] at the 6-311G(d) level as implemented in Spartan 10 software.[20] In all cases, optimised structures were confirmed by IR analyses that were characterised by the absence of any imaginary modes, hence denoting real equilibria minima. For all radical ion species, $S^2 = 0.76$, which indicates low spin contamination in all cases.[27–29] Inner-sphere reorganisation energies associated to both hole and electron transfer processes were computed utilising the widely-employed four-point method.[30–36] Inner sphere reorganisation energies on progression from neutral to radical species were calculated by subtracting the energy of the neutral species at its equilibrium geometry to that of the neutral species at the equilibrium geometry of the radical species. In turn, the inner-sphere reorganisation energies on going from the radical species to the neutral were calculated by subtracting the energy of the radical species at its equilibrium geometry to that of the radical species at the equilibrium geometry of the neutral species.

Two-dimensional dimer model system

The two-dimensional π-π dimer model system was generated employing two tetracene monomers. The geometry of the tetracene monomers was optimised using the density functional M06-2X[19] at the 6-311G(d) level as implemented in Spartan 10 software.[20]
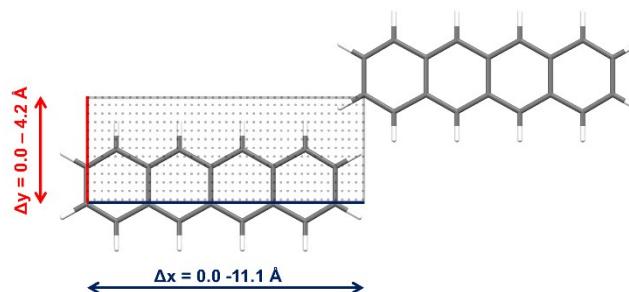
Figure 2. Illustration of the long (blue) and short (red) intermonomer displacements in the generated two-dimensional model system. Grey filled circles illustrate the location of the single point calculations through the x/y map.

The two tetracene monomers in the dimer pair were mutually aligned in a fully eclipsed fashion ($\Delta x = \Delta y = 0.0$ Å) at the optimum computed interplanar distance $\Delta z = 3.7$ Å. The top tetracene monomer was then displaced, whilst fixing the coordinates of the

bottom monomer, along the long (x) and short (y) axes simultaneously in 0.3 Å increments over a distance of 11.1 and 4.2 Å respectively as illustrated in Figure 2. The generated dimer model system bears more than 11 single point calculations per Å^2, which allows for the mapping of all substituted rubrene crystal structures reported to date (Table 1). Intermolecular interactions and transfer integrals for hole and electron at each of the 518 geometries of the model system were computed following the method described above.

Results and discussion

Intermolecular interactions and associated charge transfer integrals for reported rubrene based architectures

One-dimensional π-π stacking motifs are desirable charge propagation channels for effective charge transfer in organic semiconductors.[14,15,18] On searching the Cambridge Structural Database (CSD) for rubrene-based single crystal structures, out of the 31 reported systems, 12 were observed to conform to one-dimensional π-π slipped cofacial stacking architectures (Table 1).[7,13,37–41] Two substituted rubrene analogues, **RAGCUA** and **RAGDEL**, exhibit twisted tetracene cores as a result of the substitutions carried out on 2 of the 4 peripheral rings but were observed to also conform to the desired supramolecular stacking motif.[40] In the following, we will first focus on the in-depth analysis of those architectures bearing a planar tetracene core and then focus on structures whereby the substitutions result in twisted tetracene cores, whilst maintaining desirable one-dimensional π-π stacking motifs.

Table 1. CSD identifier, measured intermonomer displacements, intermolecular interactions, ΔE_{CP} (kJ mol^{-1}) and charge transfer integrals, t_h/t_e (kJ mol^{-1}) for π-π dimer pairs of reported rubrene based crystal structures.

CSD identifier	Δ(xyz) / Å	ΔE_{CP}	t_h/t_e
AXIDER[37]	8.43/3.47/3.76	-17.18	0.8/1.1
CIYNAB[13]	6.21/0.16/3.59	-31.83	13.3/9.0
CIYXUF[13]	6.37/0.32/3.51	-33.62	14.0/11.1
CIYYAM[13]	6.23/0.16/3.63	-29.12	13.0/7.4
INELUK02[42]	8.96/4.27/3.44	-10.71	0.4/0.4
KUSDEJ[38]	6.26/0.10/3.48	-36.66	14.9/10.6
MIVDOM[43]	6.62/0.02/3.59	-32.92	11.5/10.2
MIVDUS[43]	6.19/0.05/3.50	-38.93	14.4/9.2
PIFHIW[39]	6.32/0.16/3.50	-38.82	14.3/10.1
RAGCEK[40]	6.80/0.15/4.20	-38.60	3.8/7.4
RAGDIP[40]	7.14/0.33/3.57	-48.38	3.9/4.9
TOMVUM[41]	6.12/0.05/3.61	-36.37	12.8/7.0

It was observed that all systems in Table 1, with the exception of **INELUK02** and **RAGCEK** bear planar tetracene cores and are furthermore characterised by similar intermonomer displacements along the long and short molecular axes to those of orthorhombic rubrene (Δx/Δy/Δz = 6.18/0.30/3.64 Å). In the case of **AXIDER** and **RAGDIP**, although both exhibit planar tetracene cores, long molecular axis shifts of 8.43 and 7.14 Å were measured, respectively.

It was furthermore observed that in the eight systems exhibiting analogous displacements to those of orthorhombic rubrene (Δx, Δy and Δz of 6.18, 0.30 and 3.64 Å respectively), the largest shift along the short molecular axis is 0.32 Å, which ensures large structural overlap, critical in achieving effective wavefunction overlap and large mobilities.

Strong intermolecular interactions among the dimer pairs within the one-dimensional stacks are desirable, conferring thermal integrity to the supramolecular architecture.
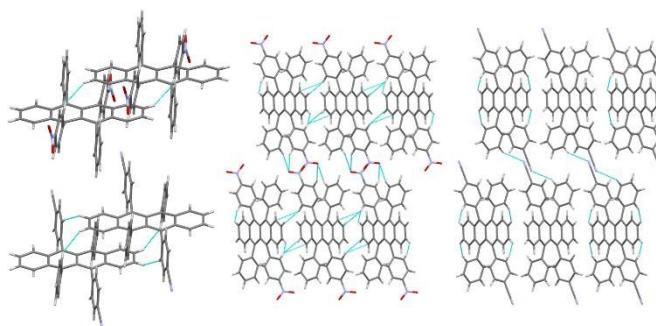

Figure 3. Short interatomic contacts involving substituents in the π-π dimer pair of **CIYNAB** (top left) and **CIYYAM** (bottom left) and crystal lattice of **CIYNAB** (centre) and **CIYYAM** (right) along the crystallographic b-axis in both cases.

The latter is of critical importance, particularly given the reported sensitivity of hole and electron transfer integrals to small (ca 1 Å) intermolecular displacements.[11,12] As a result, the strategy of enhancing these non-covalent intermolecular interactions via judicious substitutions has been widely employed in the case of rubrene and other organic conjugated systems.[10,13,21,37–41,43–45] To our surprise and contrary to the findings observed in other organic semiconductors,[12] systematic substitutions in rubrene based systems do not often result in significant changes to the computed intermolecular interactions. A common approach in trying to engineer superior analogues is to perform substitutions on the peripheral rings. However, we observe in the cases of **CIYNAB**, **CIYXUF**, **CIYYAM**, **KUSDEJ**, **MIVDOM**, **MIVDUS**, **PIFHIW** and **TOMVUM**, that modifications on the peripheral rings results in negligible changes to the computed intermolecular interactions for π-π dimer pairs. This finding can be attributed to the absence, at their exhibited intermonomer relative displacements, of close interatomic contacts involving these substituents that can lead to stabilising interactions, whereby the relative orientation of the monomers in the dimer pair is changed. In turn, the dimeric stabilisation in these architectures is ascribed to a great extent to the slipped cofacial interactions of the two tetracene cores. Nonetheless, all systems bar **CIYXUF** and **PIFHIW** exhibit enhanced lattice stabilisation via these substituents which can ultimately indirectly result in greater thermal integrity of the supramolecular π-π stacking motifs of interest. As illustrated in Figure 3, **CIYNAB** exhibits stabilising short hydrogen bonding interactions between electronegative oxygen atoms within the nitro groups and electropositive meta hydrogen atoms at 2.687 and 2.495 Å. Analogously, the cyano equivalent, **CIYYAM** exhibits a crystal lattice stabilised by close interatomic contacts between electronegative nitrogen atoms and electropositive hydrogen atoms on the meta positions of the peripheral rings at 2.596 Å.

ARTICLE

Among the various substitutions explored in crystal engineering of organic systems, isosteric replacement of hydrogen for fluorine atoms has attracted increasing interest in rubrene based systems.[38,40,41,43] Whilst both hydrogen and fluorine atoms are characterised by similar polarizabilities, their occupied volume is distinctly different.
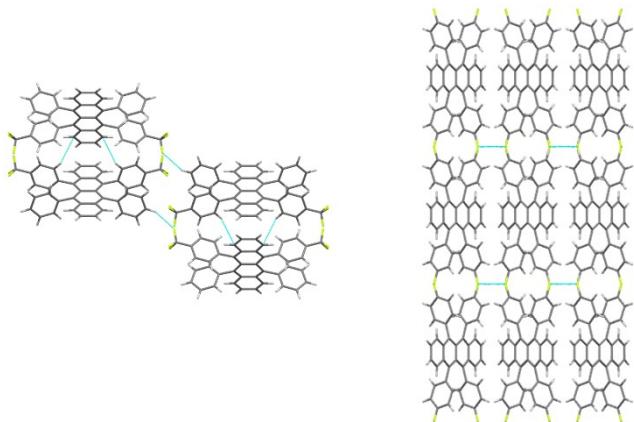

Figure 4. Short interatomic contacts in the crystal lattices of **MIVDUS** (left) and **TOMVUM** (right) along the crystallographic a and b-axes respectively.

Therefore, the physicochemical properties of systems bearing this isosteric substitution can be critically affected, such as the reversal of the electronegativity of perfluorinated rings when compared to their non-fluorinated analogues. Although inherently weak, the number of intermolecular interactions in which organic fluorine can participate (i.e. C-F---H, C-F---F-C, C-F---π_F and π-π_F) can induce significant structural changes,[46–50,50] such as the cases of diketopyrrolopyrrole based materials.[44,45] In rubrene based systems, it would be useful to rationalise the crystal lattice stabilisation in relation to the different fluorine based substitutions. The **CIYNAB/CIYYAM** trifluoromethyl substituted analogue, **CIYXUF** does not bear any close interatomic contacts in the crystal lattice involving the -CF_3 groups located at the para positions of the peripheral rings on positions 6 and 12 of the tetracene core. In turn, trifluoromethyl substitutions of the rings at positions 6 and 11 (**MIVDUS**) leads to close interatomic contacts (2.536 Å) between trifluoromethyl fluorine atoms and electropositive hydrogen atoms at the para positions of peripheral rings (Figure 4). Analogously, close C-F---F-C interatomic interactions at 2.771 Å apart were observed in **TOMVUM**, which bears fluorine substituents at the para positions of the four peripheral rings. It is anticipated that although systematic substitutions may not lead to close interatomic contacts in π-π dimer pairs, these substitutions often result in greater lattice stability which is beneficial in preserving the thermal integrity of the one-dimensional stacking motifs.
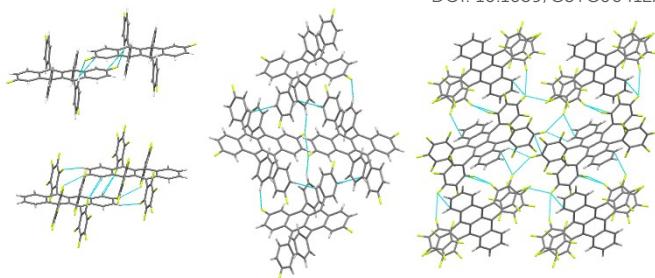

Figure 5. Short interatomic contacts involving substituents in the π-π dimer pair of **AXIDER** (top left) and **RAGDIP** (bottom left) and crystal lattice of **AXIDER** (centre) and **RAGDIP** (right) along the crystallographic a-axis in both cases.

Both **AXIDER** and **RAGDIP** exhibit planar tetracene cores and larger displacements along their long molecular axes (Δx = 8.43 and 7.14 Å respectively). In the case of **AXIDER** there is also a large short molecular axis shift (Δy = 3.47 Å). As a result, the computed intermolecular interaction for **AXIDER** is the second lowest computed (ΔE_{CP} = -17.18 kJ mol^{-1}). Interestingly, we compute the largest intermolecular interaction for **RAGDIP** (ΔE_{CP} = -48.38 kJ mol^{-1}), despite its larger intermonomer displacement along the long molecular axis. This finding can be clearly ascribed to the short interatomic contacts between electronegative organic fluorine at the meta and ortho positions of the perfluorinated peripheral rings and electropositive core hydrogen atoms at 2.644 and 2.546 Å respectively, which are enabled at the exhibited intermonomer orientation (Figure 5).

Δx/Δy = 6.18/0.30 Å   Δx/Δy = 6.80/0.15 Å
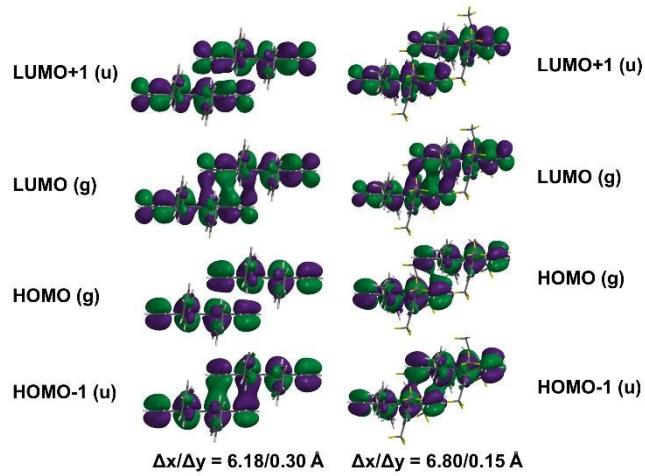
Figure 6. Illustration of the computed Kohm-Sham supramolecular orbitals of orthorhombic rubrene (left) and **RAGCEK** (right).

The remaining two systems in Table 1, namely **INELUK02** and **RAGCEK** display twisted tetracene cores. The former bears very slipped dimer pairs along both long (Δx = 8.96 Å) and short (Δy = 4.27 Å) molecular axes, resulting in negligible overlap between the tetracene cores and lowest computed interaction energy, ΔE_{CP} = -10.71 kJ mol^{-1}. The contributions to the low stabilisation energy in the dimer pair can be attributed to interatomic C-F---F-C contacts at 2.909 Å. In turn, the intermolecular interaction energy computed for **RAGCEK** is ΔE_{CP} = -38.60 kJ mol^{-1}.

Computed charge transfer integrals for holes and electrons for eight out of the 12 substituted rubrene systems in Table 1 are comparable or even superior to those computed for triclinic (t_h/t_e = 10.9/4.1 kJ mol^{-1}) and more importantly orthorhombic (t_h/t_e = 12.4/7.5 kJ mol^{-1}) rubrene forms. It is anticipated that fabrication of SC-OFETs employing these systems is warranted. The four outliers to this observed behaviour are characterised by larger intermonomer displacements and/or twisted tetracene cores, which results in lower wavefunction overlap. In this regard, critical changes to wavefunction overlap and associated computed transfer integrals on progression from orthorhombic rubrene to **RAGCEK** are observed, despite the negligible effects on the computed intermolecular interactions. These changes are manifest in a decrease in the computed hole transfer integrals whilst the integral for electron transfer remains unaltered (t_h/t_e = 12.4/7.5 and 3.8/7.4 kJ mol^{-1} for orthorhombic rubrene and **RAGCEK** respectively), which is remarkable given the small long molecular shift difference (Δx = 6.18 and 6.80 Å for orthorhombic rubrene and **RAGCEK** respectively). These changes in electronic behaviour are associated to the significant decrease in the bonding/anti-bonding character of the ungerade HOMO(-1) and gerade HOMO on progression from orthorhombic rubrene to **RAGCEK** (Figure 6) and highlight the key role played by small intermonomer displacements on the computed charge transfer integrals (vide infra) and ultimately on potential device performance.

Table 2. CSD identifier, measured intermonomer displacements, intermolecular interactions, ΔE_{CP} (kJ mol^{-1}) and charge transfer integrals, t_h/t_e (kJ mol^{-1}) for **RAGCUA** and **RAGDEL** π-π dimer pairs.

CSD identifier	Δ(xyz) / Å	ΔE_{CP}	t_h/t_e
RAGCUA[40]	7.69/0.50/4.05	-39.01	7.63/7.89
	9.04/0.05/3.79	-42.98	0.31/1.36
RAGDEL[40]	7.83/0.40/3.77	-37.89	6.58/6.94
	8.74/0.54/3.66	-44.16	0.73/0.01

RAGCUA and **RAGDEL** are both examples whereby the one-dimensional π-π stacking motif is formed by two different sets of dimer pairs arranged in a fashion A-B-A-B (Figure 7). Their monomers are characterised by twisted tetracene cores as a result of the substitutions, which significantly increase intermonomer displacements along the long molecular axis and cause a lessening of the computed hole transfer integrals compared with orthorhombic rubrene. In turn, this larger shift imparts less significance on the electron transfer integrals in dimer pairs A of **RAGCUA** and **RAGDEL**, where ambipolar charge transfer properties are predicted. Nonetheless, the significantly lower computed integrals for dimer pairs B for both systems detracts any potential interest on these systems as charge transfer mediating materials based upon their computed electronic behaviour.
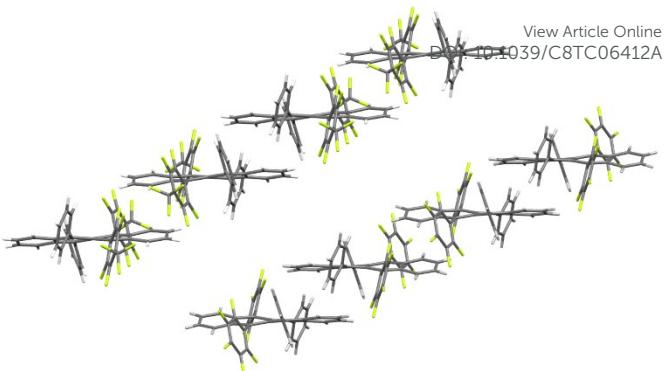

Figure 7. Illustration of the one-dimensional π-π dimer pairs in **RAGCUA** (top left) and **RAGDEL** (bottom right).

In summary, intermonomer displacements in Table 1 illustrate that irrespective of the substitution carried out, most (eight out of 12) systems exhibit shifts (Δx, Δy and Δz of 6.18, 0.30 and 3.64 Å respectively), as well as computed intermolecular interactions (ΔE_{CP} = -35.60 kJ mol^{-1}) and charge transfer integrals (t_h/t_e = 12.4/7.5 kJ mol^{-1}) which are comparable or even larger than those computed for orthorhombic rubrene. Accordingly, we anticipate that measurements in single crystals of these rubrene analogues are warranted and of interest towards development of superior alternative to the parent rubrene structure. Along these lines, it is of note that despite the negligible interest attracted by the other two known rubrene polymorphs, the triclinic form is also characterised by a supramolecular architecture where the monomers are stacked in a similar fashion to these of orthorhombic rubrene, with intermonomer displacements Δx, Δy and Δz of 5.94, 0.51 and 3.73 Å respectively, and computed intermolecular interactions (ΔE_{CP} = -35.62 kJ mol^{-1}) and charge transfer integrals (t_h/t_e = 10.9/4.1) comparable to the ones computed for its orthorhombic counterpart.

Two-dimensional π-π dimer model system

The remainder of the paper is devoted to in-depth analysis of intermolecular interactions energies and charge transfer integrals in rubrene-based π-π dimer pairs, as a function of intermonomer displacements, employing a two-dimensional model system formed by two planar tetracene monomers. Although one-dimensional model systems for tetracene have been previously reported,[34,51] herein we report for the first time a two-dimensional model system for tetracene/rubrene which allows for a greater in-depth analysis and understanding of their charge transfer properties. This two-dimensional model is important in that it dispels popular misconceptions that short molecular axis displacements are more detrimental to charge transfer than analogous ones along the long molecular axis.

Our choice of tetracene instead of rubrene for the two-dimensional model system is justified on the basis of 1) computed intermolecular interaction energies in single crystal derived π-π dimer pairs of rubrene based systems do not often depend (vide supra) on the substitutions performed on the peripheral rings and 2) the negligible extension of the FMO wavefunction density onto the peripheral rings, irrespective of the substitutions. Furthermore, and to support the choice of tetracene and not rubrene for the calculation of charge transfer integrals in our model system, we went on to calculate inner-

sphere reorganisation energies (λ) for both systems. On comparing these reorganisation energies for both hole and electron transfer process, it was observed that $\lambda_e > \lambda_h$ for both systems[43,52] and that there is a ca 2 kJ mol^{-1} increase in both $\lambda_{h/e}$ on going from tetracene to rubrene ($\lambda_{h/e}$ = 11.2/16.0 and 13.2/18.0 kJ mol^{-1} for tetracene and rubrene respectively).

Upon analysis of the 2-D model system for intermolecular interactions, it is observed that the potential energy surface (PES) for Δy = 0.0 Å is characterised by the presence of three clearly identified local minima at ca Δx = 1.5, 3.6 and 6.0 Å, coinciding with favourable local bond dipole/bond dipole and induced dipole interactions (Figure 8). We observed that whilst most investigated dimer pairs are located around the local minima at ca 6.0 Å, the π-π dimer pair of triclinic rubrene (Δy = 5.94 Å) is closest to this energetically favourable location on the PES. It is noteworthy to observe that large binding energies are not solely restricted to close short molecular axis displacements in the model system. In fact, close values to that of the global minimum (ΔE_{CP} = -42.43 kJ mol^{-1} at Δx =1.2 Å and Δy = 0.6 Å) were also observed at $\Delta x/\Delta y$ = 1.2/1.2 Å (ΔE_{CP} = -41.06 kJ mol^{-1}) and $\Delta x/\Delta y$ = 1.2/1.5 Å (ΔE_{CP} = -39.26 kJ mol^{-1}). The latter highlights that large thermal integrities of the π-π dimer pairs can be obtained at short molecular axis shifts other than Δy = 0.0 Å.
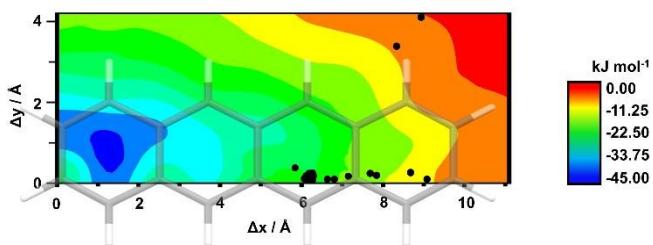

Figure 8. Three-dimensional plot of the computed intermolecular interactions as a function of the simultaneous displacements along the long (x) and short (y) molecular axes. Black filled circles denote the positions of reported rubrene-based systems.

Charge transfer integrals for both holes and electrons were computed for each single point calculation within the model system. Figure 9 illustrates larger computed transfer integrals for hole and electron at ca Δx = 0.3/3.0/6.0/9.3 and 0.3/2.1/4.5/6.6/8.7 Å respectively, which coincide in both cases with the nodal progressions for HOMO and LUMO wavefunctions. Interestingly, we observed $\Delta x/\Delta y$ regions with potential for ambipolar charge transfer behaviour and clearly distinct propagations of these regions along the short molecular axis for hole and electron transfer integrals. Consistent with the frontier molecular orbitals wavefunctions, propagation of the hole transfer integral along the short molecular axis exhibits a node at ca Δy = 1.8 Å. These observations reveal that large computed integrals for both hole and electron transfer can also be afforded in dimer pairs characterised by larger short molecular axis displacements (i.e. t_h = 13.0 and t_e = 12.6 kJ mol^{-1} computed for $\Delta x/\Delta y$ = 0.0/3.0 Å) and that dimeric systems exhibiting short molecular axis shifts should not be solely discarded. The large transfer integrals revealed by the generated model system, even for large displacements along the long/short molecular axis are anticipated to broaden the plethora of possibilities in the design,

synthesis and uses of substituted rubrene systems as charge transfer mediating materials.
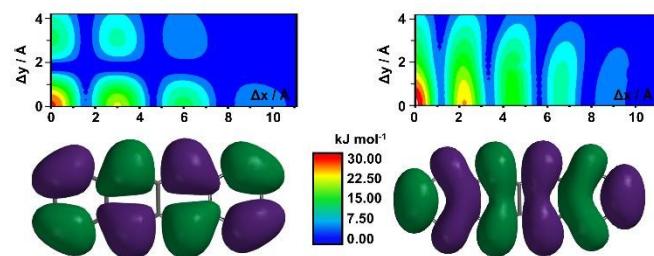
Figure 9. Three-dimensional plot of the computed hole (top left) and electron (top right) transfer integrals as a function of the displacements along the long (x) and short (y) molecular axes. Inset denotes HOMO (bottom left) and LUMO (bottom right) wavefunction for tetracene. IsoVal = 0.01.

Organic based optoelectronic materials are known for exhibiting dramatic changes on their computed charge transfer integrals upon small (ca 1 Å) intermonomer displacements. Aided by the generated two-dimensional model system, we observe that rubrene based materials also conform to these rules, with complete reversal of the t_h/t_e on going from $\Delta x/\Delta y$ = 4.5/0.0 (t_h = 2.1 and t_e = 16.8 kJ mol^{-1}) to 5.7/0.0 Å (t_h = 12.8 and t_e = 1.8 kJ mol^{-1}) as illustrated in Figure 9. In short, the gerade HOMO(-1) and ungerade HOMO supramolecular orbitals exhibit weak anti-bonding and weak bonding behaviour at $\Delta x/\Delta y$ = 4.5/0.0 Å respectively. Remarkably, the displacement of 1.2 Å along the long molecular axis lowers/rises the energy of the ungerade HOMO/gerade HOMO(-1) that now becomes HOMO(-1)/HOMO with strong bonding/anti-bonding properties. Similarly, whilst the ungerade LUMO with strong binding characteristics at $\Delta x/\Delta y$ = 4.5/0.0 Å rises its energy at $\Delta x/\Delta y$ = 5.7/0.0 Å exhibiting weak bonding behaviour, the gerade LUMO(+1) lowers its energy and exhibits a change in character from strong to weak anti-bonding upon the 1.2 Å displacement along the long molecular axis.

Lastly, we went on to test our generated model system by means of those computed charge transfer integrals for reported rubrene-based systems (vide supra). In all cases but one (**RAGDEL**), we report a successful agreement in the relative order of $t_{h/e}$ when computed charge transfer integrals for reported systems are compared to those predicted by the model system. In addition, it is striking that for all systems in Table 1 bar **AXIDER**, **RAGCEK** and **RAGDIP**, the predicted charge transfer integrals by our generated two-dimensional model system were within 10% of those computed for these π-π dimer pairs. Finally, experimental mobilities have been reported for three of the investigated systems, namely **KUSDEJ** ($\mu_{h/e}$ = 4.83/4.20 cm^2 V^{-1} s^{-1}), **MIVDOM** ($\mu_{h/e}$ = 0.07/0.01 cm^2 V^{-1} s^{-1}) and **MIVDUS** ($\mu_{h/e}$ = 0.25/0.12 cm^2 V^{-1} s^{-1}), which were observed in all cases to agree with the relative order of $t_{h/e}$ predicted by our reported model system.
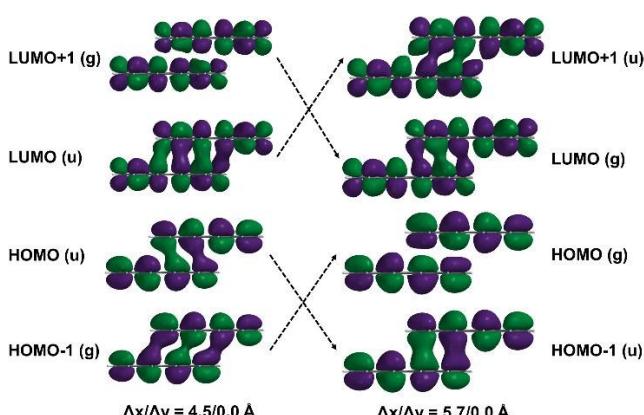
**Figure 10**. Illustration of the computed Kohm-Sham supramolecular orbitals of model system dimer pairs for Δx/Δy = 4.5/0.0 Å (left) and Δx/Δy = 5.7/0.0 Å (right). IsoVal = 0.01.

Conclusions

In conclusion, π-π dimer pairs from rubrene-based crystal structures that conform to desirable one-dimensional π-stacking motifs have been investigated in detail and their structure-property relationships extracted in an effort to aid in the crystal engineering of superior alternatives to the parent material and its polymorphs. By means of computed charge transfer integrals, we observe that large computed values are not solely restricted to dimer pairs characterised by negligible displacements along the short molecular axis and that consequently, these systems should not be discarded until experimental mobilities are carefully examined in organic single crystal field effect transistors. We observe that contrary to other organic conjugated systems, a large number of rubrene based architectures exhibit, irrespective of their molecular substitutions, similar long and short molecular axes displacements in their π-π dimer pairs, analogous to those of orthorhombic rubrene (and to a lesser extent than triclinic rubrene). Consequently, their experimental charge transfer properties ought to be investigated.

Importantly, we report a two-dimensional π-π dimer system that will allow material scientists devoted to the realisation of rubrene-based charge transfer mediating materials to screen any novel architectures by simply requiring the intermonomer displacements along the long and short molecular axes of π-π dimer pairs that conform to one dimensional stacking motifs. Underpinned by this model system, we anticipate that large hole transfer integrals can also be afforded by supramolecular motifs whereby short molecular axis displacements in the dimer pairs exceed 2 Å. In the case of electron transfer, our results reveal similar findings even for long molecular shifts beyond 6 Å. Along these lines, we envisage a large applicability of the reported model, irrespective of the substitution and intermonomer displacements.

Consequently, it is anticipated that this study can play an important role in the design and engineering of next generation rubrene based charge transfer mediating materials and that the reported system will be widely employed in screening novel architectures that conform to desirable structural motifs tailored towards efficient charge transfer.

Notes and references

1   V. Podzorov, E. Menard, A. Borissov, V. Kiryukhin, J. A. Rogers and M. E. Gershenson, *Physical Review Letters*, , DOI:10.1103/PhysRevLett.93.086602.

2   J. Takeya, M. Yamagishi, Y. Tominari, R. Hirahara, Y. Nakazawa, T. Nishikawa, T. Kawase, T. Shimoda and S. Ogawa, *Applied Physics Letters*, 2007, **90**, 102120.

3   R. Zeis, C. Besnard, T. Siegrist, C. Schlockermann, X. Chi and C. Kloc, *Chem. Mater.*, 2006, **18**, 244–248.

4   L. Huang, Q. Liao, Q. Shi, H. Fu, J. Ma and J. Yao, *Journal of Materials Chemistry*, 2010, **20**, 159–166.

5   O. D. Jurchescu, A. Meetsma and T. T. M. Palstra, *Acta Crystallographica Section B-Structural Science*, 2006, **62**, 330–334.

6   S. Bergantin, M. Moret, G. Buth and F. P. A. Fabbiani, *The Journal of Physical Chemistry C*, 2014, **118**, 13476–13483.

7   K. A. McGarry, W. Xie, C. Sutton, C. Risko, Y. Wu, V. G. Young, J.-L. Brédas, C. D. Frisbie and C. J. Douglas, *Chem. Mater.*, 2013, **25**, 2254–2263.

8   M. Mas-Torrent and C. Rovira, *Chemical Reviews*, 2011, **111**, 4833–4856.

9   D. A. Da Silva Filho, E.-G. Kim and J.-L. Brédas, *Advanced Materials*, 2005, **17**, 1072–1076.

10   J. Calvo-Castro, M. Warzecha, A. R. Kennedy, C. J. McHugh and A. J. McLean, *Crystal Growth & Design*, 2014, **14**, 4849–4858.

11   J. Vura-Weis, M. A. Ratner and M. R. Wasielewski, *Journal of the American Chemical Society*, 2010, **132**, 1738-+.

12   J. Calvo-Castro and C. J. McHugh, *Journal of Materials Chemistry C*, 2017, **5**, 3993–3998.

13   S. Uttiya, L. Miozzo, E. M. Fumagalli, S. Bergantin, R. Ruffo, M. Parravicini, A. Papagni, M. Moret and A. Sassella, *J. Mater. Chem. C*, 2014, **2**, 4147–4155.

14   M. Schwoerer and C. H. Wolf, *Organic Molecular Solids*, Wiley-VCH, 2007.

15   H. Chung and Y. Diao, *Journal of Materials Chemistry C*, 2016, **4**, 3915–3933.

16   R. Li, W. Hu, Y. Liu and D. Zhu, *Accounts of Chemical Research*, 2010, **43**, 529–540.

17   M. E. Gershenson, V. Podzorov and A. F. Morpurgo, *Reviews of Modern Physics*, 9, **78**, 973–989.

18   G. Schweicher, Y. Olivier, V. Lemaur and Y. H. Geerts, *Israel Journal of Chemistry*, 2014, **54**, 595–620.

19   Y. Zhao and D. G. Truhlar, *Theoretical Chemistry Accounts*, 2008, **120**, 215–241.

20   Y. Shao, L. F. Molnar, Y. Jung, J. Kussmann, C. Ochsenfeld, S. T. Brown, A. T. B. Gilbert, L. V. Slipchenko, S. V. Levchenko, D. P. O'Neill, R. A. DiStasio Jr., R. C. Lochan, T. Wang, G. J. O. Beran, N. A. Besley, J. M. Herbert, C. Y. Lin, T. Van Voorhis, S. H. Chien, A. Sodt, R. P. Steele, V. A. Rassolov, P. E. Maslen, P. P. Korambath, R. D. Adamson, B. Austin, J. Baker, E. F. C. Byrd, H. Dachsel, R. J. Doerksen, A. Dreuw, B. D. Dunietz, A. D. Dutoi, T. R. Furlani, S. R. Gwaltney, A. Heyden, S. Hirata, C.-P. Hsu, G. Kedziora, R. Z. Khalliulin, P. Klunzinger, A. M. Lee, M. S. Lee, W. Liang, I. Lotan, N. Nair, B. Peters, E. I. Proynov, P. A. Pieniazek, Y. M. Rhee, J. Ritchie, E. Rosta, C. D. Sherrill, A. C. Simmonett, J. E. Subotnik, H. L. Woodcock III, W. Zhang, A. T. Bell, A. K. Chakraborty, D. M. Chipman, F. J. Keil, A. Warshel, W. J. Hehre, H.

F. Schaefer III, J. Kong, A. I. Krylov, P. M. W. Gill and M. Head-Gordon, *Physical Chemistry Chemical Physics*, 2006, **8**, 3172–3191.

21 J. Calvo-Castro, M. Warzecha, I. D. H. Oswald, A. R. Kennedy, G. Morris, A. J. McLean and C. J. McHugh, *Crystal Growth & Design*, 2016, **16**, 1531–1542.

22 S. F. Boys and F. Bernardi, *Molecular Physics*, 2002, **100**, 65–73.

23 J.-D. Chai and M. Head-Gordon, *Physical Chemistry Chemical Physics*, 2008, **10**, 6615–6620.

24 A. D. Becke, *Physical Review A*, 1988, **38**, 3098–3100.

25 A. D. Becke, *Journal of Chemical Physics*, 1993, **98**, 5648–5652.

26 C. T. Lee, W. T. Yang and R. G. Parr, *Physical Review B*, 1988, **37**, 785–789.

27 A. Szabo and N. S. Ostlund, *Modern Quantum Chemistry: Introduction to Advanced Electronic Structure Theory*, McGraw-Hill, 1989.

28 A. R. Leach, *Molecular Modelling. Principles and applications*, Prentice-Hall, 2001.

29 F. Jensen, *Introduction to computational chemistry*, John Wiley and sons, 2007.

30 J. L. Bredas, D. Beljonne, V. Coropceanu and J. Cornil, *Chemical Reviews*, 2004, **104**, 4971–5003.

31 B. C. Lin, C. P. Cheng and Z. P. M. Lao, *Journal of Physical Chemistry A*, 2003, **107**, 5241–5251.

32 K. Sakanoue, M. Motoda, M. Sugimoto and S. Sakaki, *Journal of Physical Chemistry A*, 1999, **103**, 5551–5556.

33 X. Y. Li, J. Tong and F. C. He, *Chemical Physics*, 2000, **260**, 283–294.

34 V. Coropceanu, J. Cornil, D. A. da Silva Filho, Y. Olivier, R. Silbey and J.-L. Bredas, *Chemical Reviews*, 2007, **107**, 926–952.

35 W.-C. Chen and I. Chao, *The Journal of Physical Chemistry C*, 2014, **118**, 20176–20183.

36 S. F. Nelsen, S. C. Blackstock and Y. Kim, *Journal of the American Chemical Society*, 1987, **109**, 677–682.

37 Braga Daniele, Jaafari Abdelhafid, Miozzo Luciano, Moret Massimo, Rizzato Silvia, Papagni Antonio and Yassar Abderrahim, *European Journal of Organic Chemistry*, 2011, **2011**, 4160–4169.

38 W. Xie, P. L. Prabhumirashi, Y. Nakayama, K. A. McGarry, M. L. Geier, Y. Uragami, K. Mase, C. J. Douglas, H. Ishii, M. C. Hersam and C. D. Frisbie, *ACS Nano*, 2013, **7**, 10245–10256.

39 G. Schuck, S. Haas, A. F. Stassen, H. J. Kirner and B. Batlogg, *Acta Cryst. Sect. E*, 2007, **E63**, 2893.

40 W. A. Ogden, S. Ghosh, M. J. Bruzek, K. A. McGarry, L. Balhorn, V. Young, L. J. Purvis, S. E. Wegwerth, Z. Zhang, N. A. Serratore, C. J. Cramer, L. Gagliardi and C. J. Douglas, *Crystal Growth & Design*, 2017, **17**, 643–658.

41 Paraskar Abhimanyu S., Reddy A. Ravikumar, Patra Asit, Wijsboom Yair H., Gidron Ori, Shimon Linda J. W., Leitus Gregory and Bendikov Michael, *Chemistry – A European Journal*, 2008, **14**, 10639–10647.

42 Y. Sakamoto and T. Suzuki, *J. Org. Chem.*, 2017, **82**, 8111–8116.

43 K. A. McGarry, W. Xie, C. Sutton, C. Risko, Y. Wu, V. G. Young Jr., J.-L. Bredas, C. D. Frisbie and C. J. Douglas, *Chemistry of Materials*, 2013, **25**, 2254–2263.

44 J. Calvo-Castro, G. Morris, A. R. Kennedy and C. J. McHugh, *Crystal Growth & Design*, 2016, **16**, 2371–2384.

45 J. Calvo-Castro, G. Morris, A. R. Kennedy and C. J. McHugh, *Crystal Growth & Design*, 2016, **16**, 5385–5393.

46 K. Reichenbacher, H. I. Suss and J. Hulliger, *Chemical Society Reviews*, 2005, **34**, 22–30.

47 J. D. Dunitz, *Chembiochem*, 2004, **5**, 614–621.

48 J. D. Dunitz and R. Taylor, *Chemistry-a European Journal*, 1997, **3**, 89–98.

49 S. K. Nayak, M. K. Reddy, T. N. G. Row and D. Chopra, *Crystal Growth & Design*, 2011, **11**, 1578–1596.

50 D. Chopra, *Crystal Growth & Design*, 2012, **12**, 541–546.

51 S. M. Ryno, C. Risko and J.-L. Bredas, *Chemistry of Materials*, , DOI:10.1021/acs.chemmater.6b01340.

52 H. Ma, N. Liu and J.-D. Huang, *Scientific Reports*, 2017, **7**, 331.

A 2-D π-π dimer model system to investigate structure-charge transfer relationships in rubrene

Sherlyn C. Jing,[a] Callum J. McHugh [b]* and Jesus Calvo-Castro [a]*

[a] School of Life and Medical Sciences, University of Hertfordshire, Hatfield, AL10 9AB, UK.

[b] School of Computing, Engineering and Physical Sciences, University of the West of Scotland, Paisley, PA1 2BE, UK.

*Corresponding authors: j.calvo-castro@herts.ac.uk, callum.mchugh@uws.ac.uk

A two dimensional π-π model dimer system that will enable researchers to predict charge transport properties for rubrene-based materials using their single crystal π-stacking data